Reliability of VO_2-Based mmWave Switches Under 100 Million Thermal Cycles

Shangyi Chen, Mark Lust, Annie Roo, and Nima Ghalichechian, *Senior Member, IEEE*

***Abstract*—We report the lifetime investigations of the reversible phase transition vanadium dioxide (VO_2) thin film switches integrated with coplanar waveguide (CPW) under fast and direct thermal cycling. We observe that after 100 million thermal cycles, there is no degradation in the performance of VO_2 shunt switches operating at 35 – 45 GHz. S_{11} reflection coefficient as well as S_{21} transmission measurements (verified independently at both activated and inactivated states) show no statistical difference in port-to-port coupling of the VO_2 switch as a function of a cycle number. This study is enabled by the integration of Joule heaters on chip at a close proximity to a shunt VO_2 switch and a metallic CPW transmission line. Full-wave electromagnetic and multiphysics electrothermal finite element simulations are conducted to analyze the feasibility of the CPW design and the required time and power for thermal cycling. On-wafer mmWave measurements are carried out on the test vehicle after each thermal cycling phase.**

***Index Terms*—Vanadium dioxide, switch, mmWave, metal-insulator transition, reliability, thermal cycling, coplanar waveguide.**

I. INTRODUCTION

VANADIUM dioxide (VO_2) is a phase change material (PCM) which demonstrates metal-insulator transition (MIT) at a relatively low temperature of 68 °C [1]. VO_2 adopts insulating monoclinic (M1) phase below the transition temperature and metallic tetragonal rutile (R) phase above the transition temperature [2], [3]. Various approaches can be employed to induce the MIT in VO_2, such as temperature [4], electric field [5], light [6], and stress/strain [7], [8]. During the phase transition, there is a noticeable electrical resistance change by over four orders of magnitude as well as other changes in physical properties like optical transmittance. These remarkable properties, together with relatively well-developed synthesis, make VO_2 a focus of intensive investigation for numerous multifunctional devices such as electrical switches [9], microactuators [10], [11], microbolometers [12], [13], [14], [15], [16], [17], reconfigurable polarizer [18], reflectarray [19], and optical modulators [20]. Although the physical mechanics of phase transition in VO_2 have been significantly explored, it is still elusive whether the transition is dominated by Mott transition (strong electron correlation) or Peierls transformation structural phase transformation [3]. We note that Joule heating remains a variable in voltage (or current) actuation [21], [22]. When VO_2 thin film is employed in practical devices, the long-term stability or reliability of VO_2 thin films needs to be verified which can also contribute to the understanding of the driving forces and transition mechanism of VO_2 thin films.

Unfortunately, there is little literature on a lifetime study of VO_2 thin film and none exists for mmWave switches under strictly thermal cyclical loading. Other PCMs like germanium telluride (GeTe) have been exploited for RF switches in recent years which can provide latching functionality, ease of monolithic integration with other RF circuits, and reliable performance, at the cost of high activation temperatures above 750 °C [23], [24], [25]. As compared to GeTe, VO_2 is a volatile material that provides instantaneous and reversible change between two states suitable for certain RF applications. The phase transition temperature of 68° C for VO_2 is also lower than GeTe that provides advantages for certain applications. As such, the scope of this work is limited to thermal excitation of VO_2. We note that the mmWave band is defined as frequencies from 30 to 300 GHz. Understanding and quantifying the VO_2 reliability is paramount for future fifth generation (5G) and beyond communication devices such as phase shifters, switches, antennas, and intelligent surfaces.

In an early study, it was reported that the VO_2 sol-gel films' MIT switching properties driven by Joule heating effect are still unaffected after 10^8 current-voltage cycles [26]. Number of cycles by voltage or current actuation were specifically mentioned in [21], [27], [28]. In [21], two-terminal switches based on the MIT in VO_2 thin films were integrated in microwave coplanar waveguides (CPWs) in series configuration but were not tested with thermal excitation. Instead, the microwave signal transmitted through the CPW was modulated by the activation of the VO_2 switches in both voltage and current excitation modes which could by itself induce thermal effects.

Manuscript received 29 November 2022; accepted 16 January 2023. Date of publication 27 February 2023; date of current version 7 June 2023. This work was supported in part by the U.S. National Science Foundation (NSF) CAREER Award under Grant 1845370 and Grant 2149886, and in part by the Air Force Research Laboratory (AFRL)/Defense Associated Graduate Student Innovators (DAGSI) under Award RY6-OSU-19-2-AFRL2 and AFOSR Lab Task 21RYCOR019 supported by Dr. Ilya Vitebskiy. *(Corresponding author: Nima Ghalichechian.)*

Shangyi Chen was with the ElectroScience Laboratory and the Department of Mechanical and Aerospace Engineering, The Ohio State University, Columbus, OH 43212 USA. She is now with the Applied Materials, Santa Clara, CA 95054 USA (e-mail: chen.6642@osu.edu).

Mark Lust and Annie Roo are with the ElectroScience Laboratory, Department of Electrical and Computer Engineering, The Ohio State University, Columbus, OH 43212 USA (e-mail: lust.50@osu.edu; Roo.5@osu.edu).

Nima Ghalichechian is with the School of Electrical and Computer Engineering, Georgia Institute of Technology, Atlanta, GA 30308 USA (e-mail: nima.1@gatech.edu).

Color versions of one or more figures in this article are available at https://doi.org/10.1109/TDMR.2023.3249771.

Digital Object Identifier 10.1109/TDMR.2023.3249771

The lifetime of voltage and current activated VO_2 thin films' switching is demonstrated to be 16 and 260 million cycles, respectively. In another report, a field-enhanced design of 2-terminal VO_2 switches was developed [27]. A significant degradation in the VO_2 switch is observed after 2×10^5 cycles by a square wave voltage. The reliability study of VO_2/graphene/carbon nanotube film integrated in an active cloaking device capable of efficient thermal radiance control was detailed in [28]. Good reliability is established from unchanged transmittance in metallic and insulating states after 100,000 cycles of current pulses. A device undergoing voltage actuation survived 2×10^{10} cycles, but no statistical analysis, nor mmWave performance metrics were provided [22].

Although there is evidence for Joule heating in voltage actuation [3], [21], [22], literature on VO_2 reliability using all-thermal cycling is scarce. One study shows that the transition quality of the reactive sputtered VO_2 thin films is maintained without degradation after successive 102 thermal cycles [29]. No reduction in electrical resistivity contrast nor change in transition temperature were demonstrated; the authors attributed this to their high-quality polycrystalline samples and low temperature range of their fabrication process. Another example illustrates that after 60 thermal cycles, there is a broadening of transition sharpness and the width of thermal hysteresis of their VO_2 thin films by pulsed laser deposition [30]. It was suggested that large strain was accumulated around the domain boundaries during thermal cycles.

Studies on fast (milliseconds) and direct heating/cooling cycling of VO_2 thin films have not yet been reported. For materials or device reliability investigations, the common way is to analyze a figure of merit parameter indicating failure under cyclical loading. For example in [31], the thermal resistance of the Si Insulated-Gate Bipolar Transistor (IGBT) devices indicating the degradation of the solder layer was measured in each cycle. In [32], the endurance characteristics of Si:HfO_2 were investigated by obtaining the remanent polarization when the ferroelectric was exposed to a series of bipolar voltage cycles.

In this work, for the first time, we have designed a test vehicle to investigate the nature and limitations of VO_2 thin films under strictly thermal heating/cooling cycling on the order of milliseconds. It is worth noting that the reason for thermal cycling via metallic heaters is to isolate a single mechanism of actuation without concern for uncertain contribution or dominance from others. For example, there is a factor of Joule heating induced in voltage or current actuation, that raises new variables in the VO_2 transition that are not experimentally controlled [21], [22]. Here, VO_2 thin film is integrated in CPW for analyzing the RF performance when at insulating and metallic states. The insulating phase is referred to as an inactive state in this manuscript, however, it is commonly called dielectric, semiconductor, or cold state. In contrast, the metallic phase is referred to an active state in this manuscript. The Joule heaters are designed and integrated adjacent to VO_2 thin film to locally heat through the phase transition region without degrading the RF performance of the switch. The RF port-to-port measurements of the CPW structure are carried out. Additionally, the heating and passive cooling capabilities of the Joule heaters are verified with the simultaneous RF measurements. After increasing durations of thermal cycling, the S-parameter data is utilized to analyze the failure or degradation of VO_2 thin film up to 100 million cycles. MmWave port-to-port measurements are performed after 0, 10^5, 10^6, 10^7, and 10^8 cycles, respectively. This work discusses reliability study of VO_2 thin film and does not attempt to display state-of-the art switch performance.

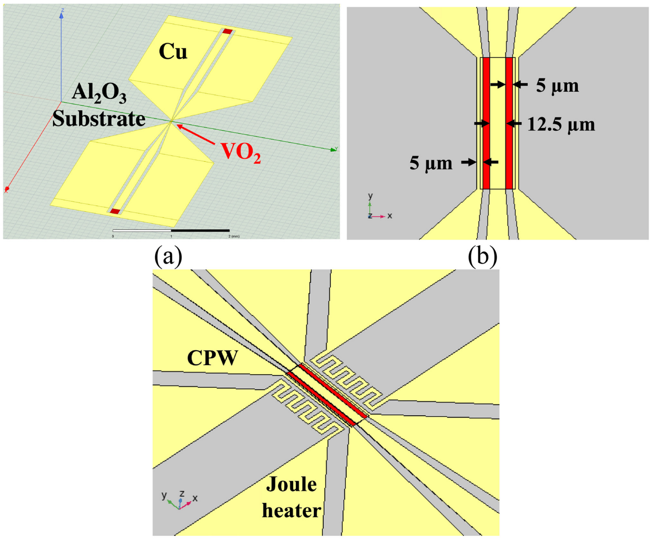

(a) (b) (c)

Fig. 1. VO_2 mmWave switch (a) 3D overview, (b) top view of the CPW-based test vehicle with a shunt VO_2 switch, and (c) a VO_2 shunt switch and two parallel Joule heaters.

This manuscript is structured as follows. The design of the CPW shunt switch and full-wave simulation results followed by electrothermal simulations are discussed in Section II. The fabrication process for the test vehicle on a sapphire substrate is reported in Section III. Measurement results including static characterization of the VO_2 switch, verification of the thermal cycling, and cyclical loading tests are discussed in Section IV followed by a conclusion in Section V.

II. DESIGN

The CPW structure consists of a center signal line surrounded by a ground plane on a sapphire substrate (loss tangent $\delta = 0.0001$, relative permittivity $\varepsilon_r = 9.3$). The state-of-the-art deposition of VO_2 thin film is on single crystal sapphire substrates [33] because of the strong lattice match between the C-plane sapphire and VO_2. In our previous study [1], we were able to deposit VO_2 on sapphire with a sharp change in resistivity (9.76×10^4), which makes VO_2 an ideal material for a shunt RF switch. In that study, we also deposited VO_2 on Si with annealed Al_2O_3 buffer layers with resistivity contrast ratio of 1.46×10^4. Sapphire is used in this work for its higher performance VO_2 and ease of fabrication. In our test vehicle, we employ shunt switch architecture comprising a rectangular patch of VO_2 spanning the gap between signal line and two ground lines of the CPW transmission line. Fig. 1 (a) shows the 3D schematic of the designed test vehicle. Top view schematic of the switch and CPW line are shown in Fig. 1 (b). The center line width, ground line width, and the gap of the CPW are 12.5 µm, 5 µm, and 5 µm, respectively. VO_2 size is 22.5 µm × 100 µm connecting the signal

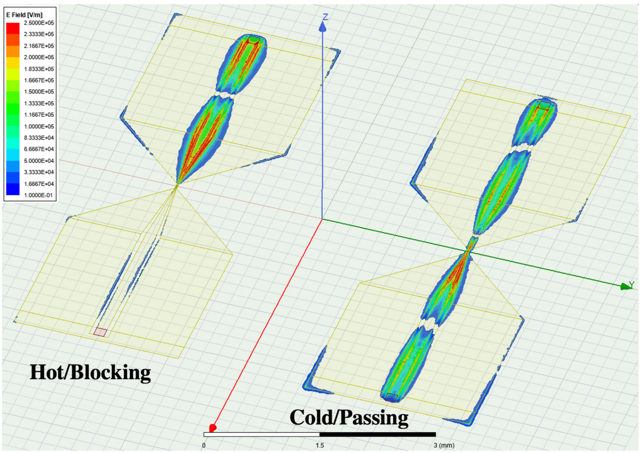

Fig. 2. Electric field simulated for the CPW with VO_2 switch at activated (left) and inactivated (right) states.

line to the ground on the two sides (shunt). To switch between insulating and metallic states of VO_2 thin film, we use two parallel Joule heaters as demonstrated in Fig. 1 (c). Two heaters, routed to be electrically parallel, are designed symmetrically for each RF switch. For efficient thermal coupling between heaters and the VO_2 switch, metal areas are removed from the ground line.

A. Electromagnetic Simulation

Full wave electromagnetic simulations are carried out using ANSYS HFSS. Fig. 2 shows the RF signal transmission characterizations of the designed CPW. When VO_2 is at the inactivated state (insulating phase), RF signals can pass through. While VO_2 is at the activated state (metallic phase), the signal line is short-circuited to the ground and RF signal is fully reflected. The simulated S_{11} and S_{21} at 35 – 45 GHz are illustrated in Fig. 3 (a) and (b), respectively, for inactivated and activated states. At the inactivated state, port-to-port coupling or S_{21} is approximately −2.0 dB. In contrast, S_{21} ranges from −9.6 dB to −42 dB at the activated state. Likewise, at the inactivated state, the reflection coefficient or S_{11} ranges from −37 dB to −13 dB. In contrast, S_{11} is approximately −2.4 dB at the activated state. For this study, stark difference between the two switch states provides a benchmark for tracking the phase of the VO_2 at mmWave frequencies.

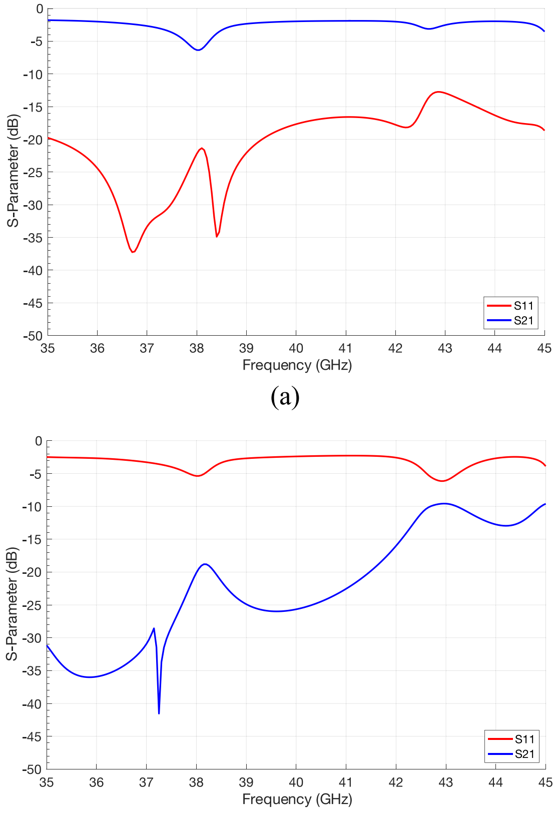

(a)

(b)

Fig. 3. Full-wave simulation results S_{11} and S_{21} at 35 – 45 GHz for VO_2's (a) inactivated and (b) activated states.

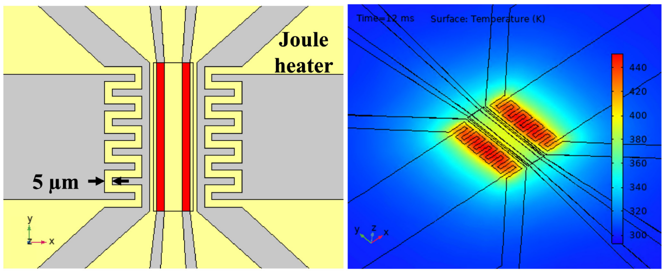

(a) (b)

Fig. 4. (a) Joule heater design; (b) temperature profile of the VO_2 switch when excited using a thermal Joule heater. The temperature scale is from 290 to 450 °C.

B. Electrothermal Simulation

In this work, the insulating and metallic states of VO_2 are switched by employing two parallel Joule heaters. The thermal cycling frequency is related to the VO_2 shunt switch and Joule heaters designs. There are a few challenges in the Joule heater design: the energy provided by the Joule heater needs to be concentrated around VO_2; fast thermal cycling is required; and the dimension limitations in the fabrication must be considered. To simplify the fabrication process for the test vehicle, copper (Cu) is chosen as the material of choice for both the heater as well as the CPW transmission line. One-step fabrication process for metal deposition and patterning shared between the CPW lines and heaters significantly simplifies the prototyping process. The high electrical conductivity (5.98×10^7 S/m) of Cu does provide a challenge for the heater design. Therefore, a meandered heater layout with a narrow width are chosen. The heater is designed using serpentine traces with a small width of 5 µm and a separation of 5 µm around the VO_2 thin film as shown in Fig. 4 (a). The smaller width as compared to the traces results in a larger electrical resistance and thermal power concentration around the VO_2 switches. Furthermore, a short response time is needed to enable testing millions of cycles in a reasonable time.

To optimize the Joule heater design and calculate the required electrical power, duty cycle, and temperature distribution, COMSOL Multiphysics is used with the Heat Transfer and AC/DC modules. When applying a voltage to the Joule heater, the current is calculated by the AC/DC module. The generated heat energy is then coupled to the Heat Transfer

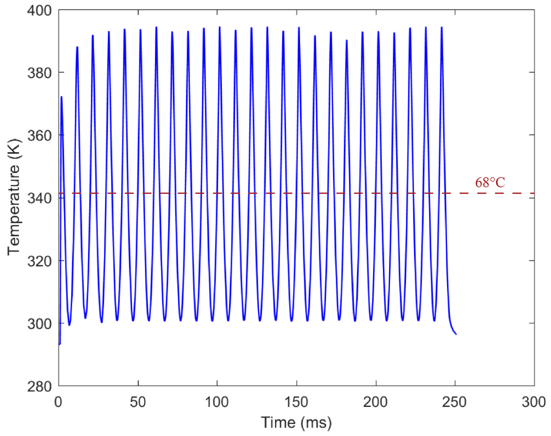

Fig. 5. Time domain thermal simulation results for the cyclical excitation. The phase transition temperature is marked with a dashed line. Temperatures above the line indicate metallic state corresponding to the activated switch. Temperatures below the line indicate insulating state corresponding to the inactivated switch.

TABLE I
DEPOSITION CONDITION OF DC SPUTTERED VO_2 THIN FILM

Parameter	Value
Ar gas flow (sccm)	19.96
O_2 gas flow (sccm)	1.58
Temperature (°C)	650
Pressure (mTorr)	10
Power (W)	250

module to analyze the temperature distribution. The temperature for the bottom surface of the sapphire substrate is set to 293 K. The constant convective heat flux density of 5 W/m^2K is defined for the remaining surfaces. In addition to convective cooling, the heat transfer between Joule heaters, VO_2, and sapphire is dominated by thermal conduction. Multiple cycles of pulses with 6.5 V for 1 ms and 0 V for 9 ms (10% duty cycle) are applied to the parallel Joule heaters. Fig. 4 (b) demonstrates the simulated temperature profile at the activated state. It is shown that the VO_2 pattern can be efficiently and locally heated by the surrounding traces. The dynamic response for the cyclical excitation of the VO_2 thin film is shown in Fig. 5 validating operation below and above the phase transition temperature of 68 °C or 341 K. This thermal cycling of the thin film is repeatable with the specified applied pulse. The VO_2 is heated to ~400 K and cooled down to ~300 K. The extracted current is 0.4 A for each heater, or 0.8 A per pair.

III. FABRICATION

A two-layer photolithography process for the proposed test architectures is developed and is illustrated in Fig. 6. VO_2 thin film is deposited by DC sputtering (AJA Orion RF/DC Sputter Deposition Tool) on a 2-inch C-plane sapphire substrate with a thickness of 430 μm. A high-purity vanadium target is used in a mixed Ar/O_2 environment. The deposition parameters including the optimized Ar/O_2 gas ratios are listed in Table I, and were detailed in our previous work [1]. The measured resistivity of deposited 107-nm-thick VO_2 on sapphire using a 4-point probe is shown in Fig. 7 [1]. The resistivity contrast ratio between insulating and metallic states is 9.76×10^4. Parallel-beam x-ray diffraction (XRD) was used to determine VO_2's crystal structure. Atomic force microscopy (AFM) and scanning electron microscopy (SEM) were also used to analyze properties of VO_2. The deposited 107-nm-thick VO_2 thin film is then patterned for the integration with the CPW structure. The sample is primed with HMDS adhesion promoter. Next, 1.4-μm-thick photoresist Shipley S1813 is spin coated and patterned. VO_2 thin film is dry etched in an inductively coupled plasma reactive ion etching (ICP RIE) system (Plasma Therm SLR770) with gas Ar/SF_6. The RIE recipe is given in Table II. The CPW structure and Joule heaters are fabricated by the lift-off process with a 250-nm-thick Cu layer. To facilitate this process, negative photoresist AZ nLOF2020 with a thickness of 1.8 μm is deposited and patterned. Note that, to improve the adhesion of the metal layer, a 30-second oxygen plasma is utilized to remove remaining photoresist residue after development. The e-beam evaporation process

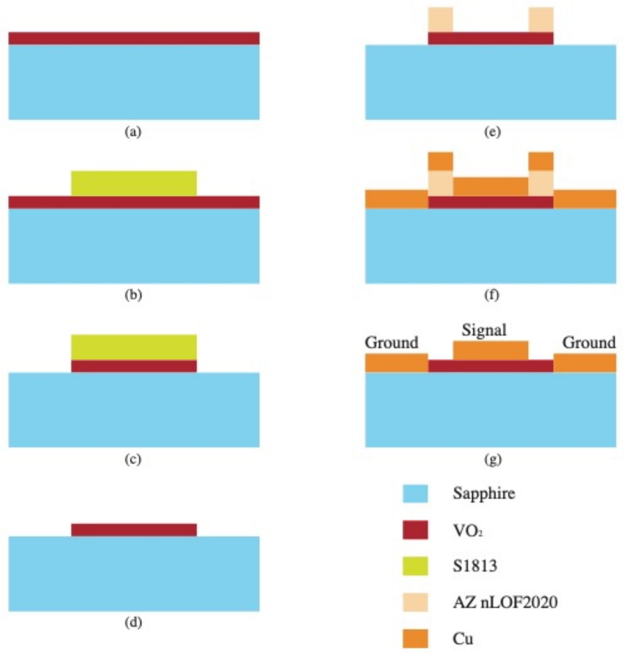

Fig. 6. Fabrication steps of the CPW-based test vehicle: (a) VO_2 sputtering, (b) positive photoresist S1813 patterning, (c) VO_2 RIE, (d) S1813 stripping, (e) negative photoresist AZ nLOF2020 patterning, (f) Cu e-beam evaporation, and (g) lift-off.

TABLE II
RIE RECIPE OF VO_2 THIN FILM

Parameter	Value
Ar gas flow (sccm)	20
SF_6 gas flow (sccm)	20
Temperature (°C)	20
Pressure (mTorr)	5
RIE power (W)	100

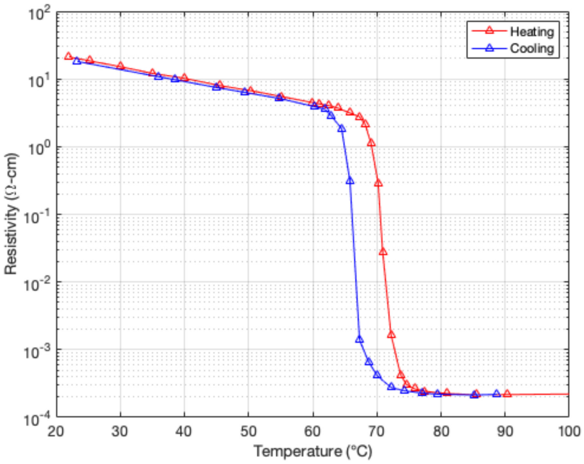

Fig. 7. Measured resistivity versus temperature of VO_2 thin films on C-plane sapphire substrate.

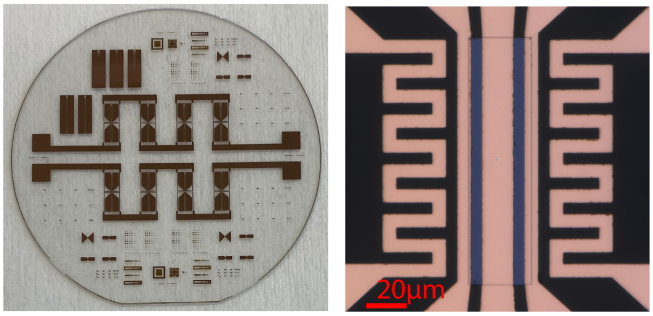

(a) (b)

Fig. 8. Fabricated DUTs (a) full wafer and (b) micrograph of VO_2 shunt switch.

is performed to deposit a Cu layer (Denton DV 520A electron gun thermal evaporator). First, a thin titanium layer of 10 nm is deposited with a rate of 2.4 Å/s to improve the Cu adhesion. Next, a 250-nm-thick Cu layer is deposited with a rate of 1.9 Å/s. Finally, N-Methyl-2-Pyrrolidone (NMP) at 80 °C for 20 minutes is used for lift-off. Fig. 8 shows the fabricated device. There are two symmetric sets of testing vehicles; each set consists of four devices under test (DUT). The Joule heater pairs associated with each DUT are connected in series with separate DC Cu traces.

IV. MEASUREMENTS

The fabricated samples are characterized to verify the thermal cycling and investigate the reliability of the VO_2 thin film.

A. Static Characterization of VO_2 Shunt Switch

The RF port-to-port measurements are carried out on a Cascade M150 probe station shown in Fig. 9 (a). Prior to RF measurements, probes are conditioned on a cleaning substrate and then calibrated using a standards substrate. The test is performed in a temperature-controlled laboratory environment at standard room temperature with variation within a few degrees Celsius (∼19-21 °C) that is significantly smaller and outside of the transition temperature of VO_2. As such, any small fluctuations in the testing environment will have no significant effects on the measured data. The S-parameters of the VO_2 shunt switch at different states of VO_2 are measured using a 67 GHz phase network analyzer (PNA) and ground-signal-ground (GSG) 65 GHz probes (Air Coplanar Probe from FormFactor). By applying a constant voltage to the Joule heaters, the activated state of VO_2 is obtained. The voltage is applied to the two pads of the Joule heaters through the DC probes connected to a Keysight B2962A power source as shown in Fig. 9 (a) and (b). Fig. 10 (a) demonstrates measurement results of S-parameters with VO_2 at the inactivated state. The measured frequency range is from 35 to 45 GHz. S-parameters are measured giving S_{21} from −4.0 dB to −1.6 dB and S_{11} from −48 dB to −12 dB across the full frequency range. These moderate S_{21} values are attributed to non-ideal ground planes and surrounding metal structures on the wafer. While the specific insertion loss of the switch performance is not production-ready, the comparison of switching performance across many thermal cycles is just as insightful for determining reliability as in complex, highly-optimized switches. The activated state of VO_2 is achieved by employing DC voltage to the heaters. The RF measurements are conducted simultaneously with DC activation voltage of 15 V as demonstrated in Fig. 10 (b) with S_{11} from −6.2 dB to −3.3 dB and S_{21} from −59 dB to −17 dB. There is also some rippling present due to factors that cannot be controlled for in calibration such as normal probe positioning and wear.

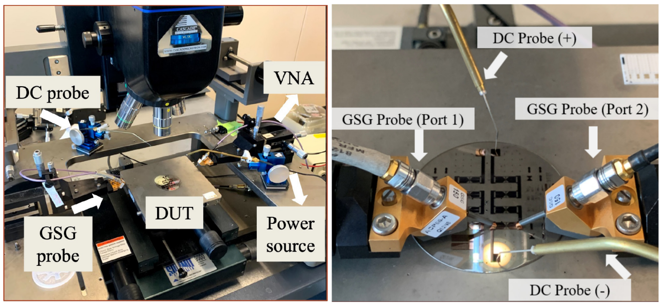

(a) (b)

Fig. 9. Probe station test setup for the VO_2 shunt switch characterization: (a) overview and (b) close-up of DC and GSG probes contacting the heater pads and the DUT CPW pads, respectively.

During hysteresis measurements, the DC voltage is ramped up from 0 V to 15 V then ramped down to 0 V. S-parameter measurements are taken at 0.5 V intervals. Fig. 11 illustrates the overall S-parameter data at 38 GHz that is changed with applied voltage. The hysteresis measurement given is taken from a different sample from the frequency sweep shown in Fig. 10, so the exact values may vary. The VO_2's MIT begins at a heater voltage of 12.3 V DC and reaches maximum reflection at 13.5 V and minimum transmission at 15 V. S_{11} increases from −35 dB at 0 V to −4.0 dB at 13.5 V. Similarly, S_{21} decreases from −3.0 dB at 0 V to −39 dB at 15 V. As expected, hysteresis is observed as the VO_2 transitions back to insulating phase with S_{11} beginning to fall at 12.4 V and settling at 11.2 V; S_{21} began to rise again at 13.8 V,

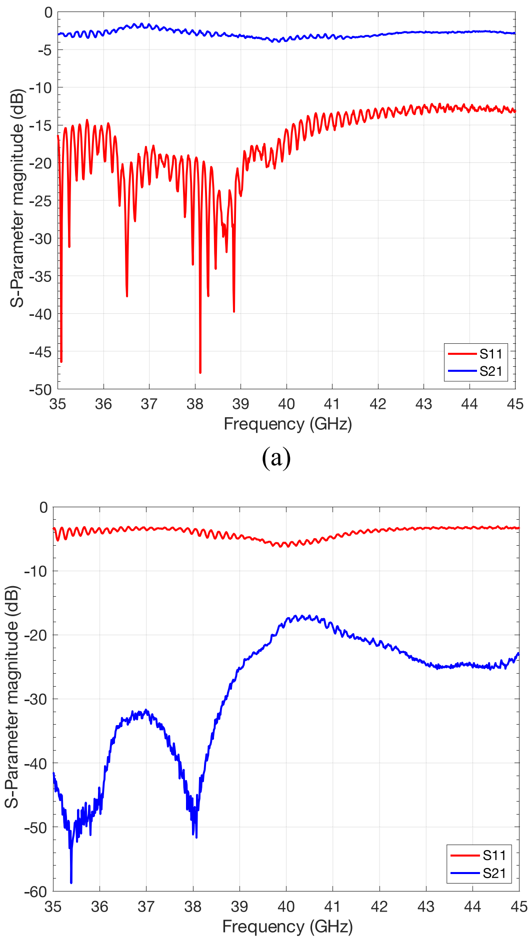

(a)

(b)

Fig. 10. S_{11} and S_{21} measurement results with VO_2 at (a) inactivated state with 0 V DC applied to the Joule heaters and (b) activated state with 15 V DC applied.

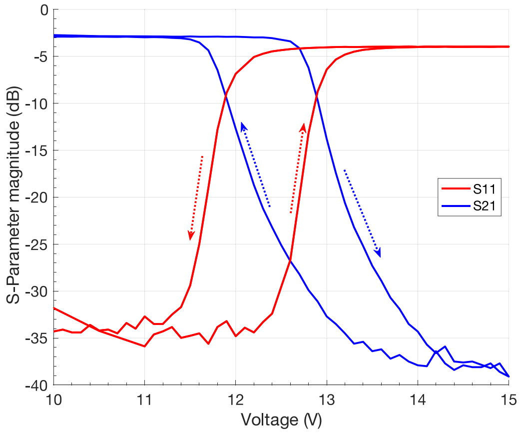

Fig. 11. Measured S-parameters at 38 GHz with ramped DC voltage applied to the heaters.

settling at 11.2 V. The result is a hysteresis loop 1.1 V wide. The total resistance for the set of four heater pairs is 38.3 Ω. Corresponding maximum power is 5.87 W at peak voltage of 15 V for the set of four DUTs and 1.47 W per switch.

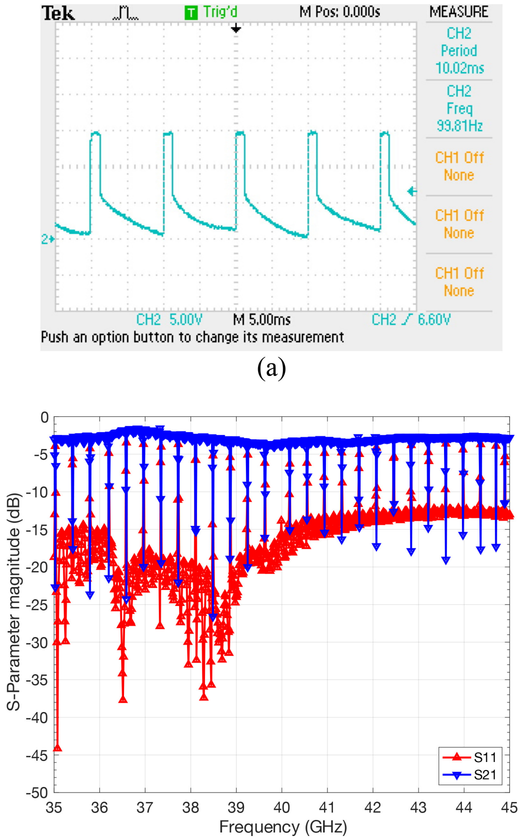

(a)

(b)

Fig. 12. (a) Measured PWM signal for thermal cycling showing duty cycle of 10% at 100 Hz and 15 V_{pp}; (b) measured transient S_{11} and S_{21} values during thermal cycling.

B. Verification of Thermal Cycling

The thermal cycling is tested by measuring S-parameters when applying voltage pulses to the Joule heaters. An Arduino Uno outputs a 100 Hz signal, 10% duty cycle pulse-width modulated (PWM) waveform to a power amplifier that steps up the Arduino's output from 5 V_{pp} to 15 V_{pp}. To verify the PWM operation, an oscilloscope is attached to the DC probes and confirmed that the switching for thermal cycling is as expected. The resulting PWM waveform is sent through DC probes contacting the pads of the Joule heaters on the wafer, while sweeping the 35 – 45 GHz range using PNA at IF bandwidth of 1 kHz to capture the repeated switching transition. With the 100 Hz PWM wave, the switch cycles approximately 14 times per PNA sweep. The two steps are illustrated in Fig. 12 and verify that indeed the thermal cycling of the switch causes real-time change in S-parameter of the transmission line.

C. Reliability Characterization

The activated and inactivated states of VO_2 are thermally cycled for a total of 100 million times. Then, S-parameter values of the activated and inactivated states of the VO_2 are measured at the cycle numbers of 0, 10^5, 10^6, 10^7, and 10^8, respectively. S-parameter data, across the measured frequency band of 35 – 45 GHz, for each of the four DUTs are measured

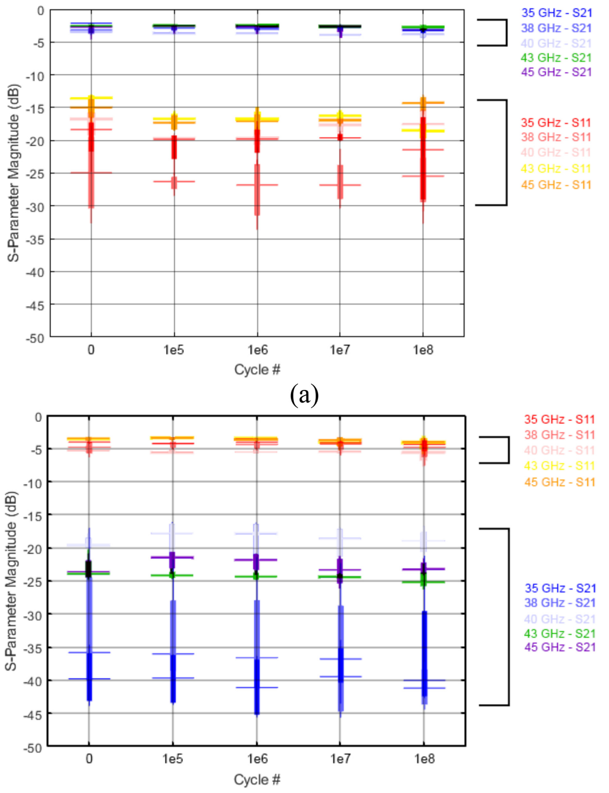

(a)

(b)

Fig. 13. Box and whisker plot of (a) S_{11} and S_{21} measurements of the inactivated states and (b) the activated states of the 4 DUTs from cycles 0 to 10^8. Data is shown for 5 frequencies from 35 to 45 GHz. S_{11} and S_{21} are marked on the side.

after cycling with its activated and inactivated states. Measured values are shown in Fig. 13 (a) and Fig. 13 (b), for inactivated and activated states, respectively. It is observed that while there are expected variation in the whiskers of the plot due to the variation of S-parameter data between each of the DUTs, there are no significant differences between each of the cycles ranging from 0 to 100 million. The differences in exact S-parameter values at the same thermal cycle are attributed to the factors mentioned in the previous subsection that cause the rippling and to small differences in surrounding geometry.

To verify our hypothesis, a Paired T-Test analysis is performed. This is done to quantitatively determine if there are any statistical differences between the S-parameter data to indicate degradation in the VO_2. The null hypothesis of (1) states that there is no difference in the means of each S-parameter of each DUT (as the number of thermal cycles increases) indicating lack of degradation in the VO_2 material; accordingly, the alternative hypothesis of (2) states that there is a difference in the means of the S-parameters of each DUT as the number of cycles increases, thereby indicating some form of degradation in the VO_2 switch over the course of thermal cycling. Here, μ_0 is the mean S-parameter value at zero cycles and μ_x is the mean S-parameter value at 10^5, 10^6, 10^7, and 10^8, switching cycles:

$$H_0\colon \mu_{0\ cycles} - \mu_{\mathrm{x\ cycles}} = 0, \tag{1}$$

$$H_a\colon \mu_{0\ cycles} - \mu_{\mathrm{x\ cycles}} \neq 0. \tag{2}$$

TABLE III
PAIRED T-TEST RESULTS FOR S-PARAMETER CYCLE COMPARISONS AT 38 GHz

Cycles under Comparison	H and P values
0 cycles & 10^5 cycles	H=0, P=0.5386
0 cycles & 10^6 cycles	H=0, P=0.0166
0 cycles & 10^7 cycles	H=0, P=0.3154
0 cycles & 10^8 cycles	H=0, P=0.2943

The Paired T-Test is run comparing the S-parameter results at 0 cycles and each of the consecutive cycles to determine if any significant differences exist at a 1% significance level between the four DUTs before and after thermal cycling. The S-parameters for 5 frequencies from 35 to 45 GHz have similar degradation, and the corresponding H and P values for the various cycle comparisons at 38 GHz are shown in Table III.

The P-value of the test indicates the likelihood of data occurring under the null hypothesis. For our test, this states that there is statistically no significant difference between the S-parameter values of the DUTs between each consecutive cycle. At the 1% significance level, the threshold for the P-value is 0.01. A P-value <1% would be statistically significant, meaning a failure of the null hypothesis. We saw no statistically significant results, meaning the null hypothesis passes all tests. Consequently, the resulting H-value of each comparison test equates to 0, thereby stating that the null hypothesis is true and that there are no statistically significant differences between the S-parameters of consecutive cycles beyond 0.

This translates to no significant degradation or change in the performance of VO_2 even after 100 million thermal cycles. The proposed VO_2 shunt switch with localized Joule heaters is the first step to exploit the reliability performance of this material for RF applications. Future studies could include expanded frequency range as well as implantation of a series switches with more efficient embedded heaters such as nichrome, molybdenum, or tungsten.

V. CONCLUSION

In this work, for the first time, we investigate the reliability of VO_2 thin film switches under prolonged rapid all-thermal actuation using localized Joule heaters and CPW shunt switch. The RF port-to-port measurements of the VO_2 shunt switch are performed at inactivated and activated states, with S_{21} of −4.0 dB −1.6 to and −59 dB to −17 dB, and S_{11} of −48 dB to −12 dB and -6.2 dB to −3.3 dB, respectively, across 35 – 45 GHz. The strongest switching performance occurred at 38 GHz with S_{21} of −2.4 dB and −38 dB and S_{11} of −23.7 dB and −4.1 dB, at inactivated and activated states, respectively. The timing and reliability of the thermal cycling are verified using the pulse voltage and oscilloscope; the switching is also verified at mmWave band of 35 – 45 GHz. Even after 100 million cycles, statistical analysis of S-parameter measurements gives no indication of degradation in electrical properties the VO_2 switches. The study was concluded after the 100 million cycles, having observed no device degradation or failure. Power handling and linearity of the switch may be important in certain applications; however, these were not a part of our study. We also note that for certain applications such as space, a temperature-controlled environment can enable application of VO_2 switches well above the phase transition temperature. The reported measurement results indicate high reliability of VO_2 switches under cyclical testing and provide confidence for development of future optimized switches for next generation mmWave devices for 5G and beyond applications.

REFERENCES

[1] M. Lust, S. Chen, C. E. Wilson, J. Argo, V. Doan-Nguyen, and N. Ghalichechian, “High-contrast, highly textured VO2 thin films integrated on silicon substrates using annealed Al2O3 buffer layers,” *J. Appl. Phys.*, vol. 127, no. 20, 2020, Art. no. 205303, doi: 10.1063/1.5144816.

[2] J. B. Goodenough, “The two components of the crystallographic transition in VO_2,” *J. Solid State Chem.*, vol. 3, no. 4, pp. 490–500, 1971, doi: 10.1016/0022-4596(71)90091-0.

[3] R. Shi et al., “Recent advances in fabrication strategies, phase transition modulation, and advanced applications of vanadium dioxide,” *Appl. Phys. Rev.*, vol. 6, no. 1, 2019, Art. no. 11312, doi: 10.1063/1.5087864.

[4] M. M. Qazilbash et al., “Mott transition in VO_2 revealed by infrared spectroscopy and nano-imaging,” *Science*, vol. 318, no. 5857, p. 1750, 2007, doi: 10.1126/science.1150124.

[5] H.-T. Kim, B.-G. Chae, D.-H. Youn, G. Kim, and K.-Y. Kang, “Raman study of electric-field-induced first-order metal-insulator transition in VO_2-based devices,” *Appl. Phys. Lett.*, vol. 86, no. 24, 2005, Art. no. 242101, doi: 10.1063/1.1941478.

[6] A. Cavalleri et al., “Femtosecond structural dynamics in VO_2 during an ultrafast solid-solid phase transition,” *Phys. Rev. Lett.*, vol. 87, no. 23, 2001, Art. no. 237401, doi: 10.1103/PhysRevLett.87.237401.

[7] J. Cao et al., “Strain engineering and one-dimensional organization of metal–insulator domains in single-crystal vanadium dioxide beams,” *Nat. Nanotechnol.*, vol. 4, no. 11, pp. 732–737, 2009.

[8] H. Bin et al., “External-strain induced insulating phase transition in VO_2 nanobeam and its application as flexible strain sensor,” *Adv. Mater.*, vol. 22, no. 45, pp. 5134–5139, 2010, doi: 10.1002/adma.201002868.

[9] C. Hillman, P. Stupar, and Z. Griffith, “VO2 switches for millimeter and submillimeter-wave applications,” in *Proc. IEEE Compound Semicond. Integr. Circuit Symp. (CSICS)*, 2015, pp. 1–4.

[10] H. Ma et al., “Flexible, all-inorganic actuators based on vanadium dioxide and carbon nanotube bimorphs,” *Nano Lett.*, vol. 17, no. 1, pp. 421–428, 2017, doi: 10.1021/acs.nanolett.6b04393.

[11] K. Liu, C. Cheng, Z. Cheng, K. Wang, R. Ramesh, and J. Wu, “Giant-amplitude, high-work density microactuators with phase transition activated nanolayer bimorphs,” *Nano Lett.*, vol. 12, no. 12, pp. 6302–6308, 2012, doi: 10.1021/nl303405g.

[12] C. D. Reintsema, E. N. Grossman, and J. A. Koch, “Improved VO_2 microbolometers for infrared imaging: Operation on the semiconducting-metallic phase transition with negative electrothermal feedback,” in *Proc. Infrared Technol. Appl. XXV, SPIE*, vol. 3698, Jul. 1999, pp. 190–201. [Online]. Available: https://doi.org/10.1117/12.354520

[13] S. Chen, M. Lust, and N. Ghalichechian, “Exploiting nonlinear properties of VO_2 in a mmWave antenna-coupled sensor,” in *Tech. Dig. Solid-State Sensor Actuator Workshop*, Hilton Head Island, SC, USA, 2022, pp. 1–4.

[14] S. Chen, M. Lust, and N. Ghalichechian, “Multiphysics simulation of hypersensitive microbolometer sensor using vanadium dioxide and air suspension for millimeter wave imaging,” *Microsyst. Technol.*, vol. 27, no. 7, pp. 2815–2822, 2021, doi: 10.1007/s00542-020-05031-0.

[15] S. Chen, M. Lust, and N. Ghalichechian, “A vanadium dioxide microbolometer in the transition region for millimeter wave imaging,” in *Proc. IEEE Int. Symp. Antennas Propag. USNC-URSI Radio Sci. Meeting*, 2019, pp. 1641–1642, doi: 10.1109/APUSNCURSINRSM.2019.8888891.

[16] S. Chen, B. Ghassemiparvin, and N. Ghalichechian, “The design of high-responsivity millimeter wave imager using vanadium dioxide microbolometers,” in *Proc. 12th Eur. Conf. Antennas Propag. (EuCAP)*, London, U.K., 2018, pp. 1–4, doi: 10.1049/cp.2018.0560.

[17] S. Chen, M. Lust, and N. Ghalichechian, “Antenna-coupled microbolometer based on VO_2’s non-linear properties across the metal–insulator transition region,” *Appl. Phys. Lett.*, vol. 121, no. 20, 2022, Art. no. 201901, doi: 10.1063/5.0123779.

[18] M. Lust and N. Ghalichechian, “VO2-based reconfigurable meanderline polarizer at Ka-band,” in *Proc. IEEE Int. Symp. Antennas Propag. USNC-URSI Radio Sci. Meeting (APS/URSI)*, Singapore, Dec. 2021, pp. 551–552, doi: 10.1109/APS/URSI47566.2021.9704350.

[19] J. Ramsey, K. Henderson, and N. Ghalichechian, “Thermally actuated vanadium dioxide millimeter wave reflectarray,” in *Proc. 16th Eur. Conf. Antennas Propag. (EuCAP)*, Madrid, Spain, 27 Mar./Apr. 2022, pp. 1–3, doi: 10.23919/EuCAP53622.2022.9768925.

[20] D. Lee et al., “Sharpened VO_2 phase transition via controlled release of epitaxial strain,” *Nano Lett.*, vol. 17, no. 9, pp. 5614–5619, 2017, doi: 10.1021/acs.nanolett.7b02482.

[21] A. Crunteanu et al., “Voltage- and current-activated metal–insulator transition in VO_2-based electrical switches: a lifetime operation analysis,” *Sci. Technol. Adv. Mater.*, vol. 11, no. 6, 2010, Art. no. 65002, doi: 10.1088/1468-6996/11/6/065002.

[22] I. P. Radu et al., “Switching mechanism in two-terminal vanadium dioxide devices,” *Nanotechnology*, vol. 26, no. 16, 2015, Art. no. 165202, doi: 10.1088/0957-4484/26/16/165202.

[23] N. El-Hinnawy et al., “A four-terminal, inline, chalcogenide phase-change RF switch using an independent resistive heater for thermal actuation,” *IEEE Electron Device Lett.*, vol. 34, no. 10, pp. 1313–1315, Oct. 2013, doi: 10.1109/LED.2013.2278816.

[24] T. Singh and R. R. Mansour, “Loss compensated PCM GeTe-based latching wideband 3-bit switched true-time-delay phase shifters for mmWave phased arrays,” *IEEE Trans. Microw. Theory Techn.*, vol. 68, no. 9, pp. 3745–3755, Sep. 2020, doi: 10.1109/TMTT.2020.3007833.

[25] T. Singh and R. R. Mansour, “Experimental investigation of performance, reliability, and cycle endurance of nonvolatile DC–67 GHz phase-change RF switches,” *IEEE Trans. Microw. Theory Techn.*, vol. 69, no. 11, pp. 4697–4710, Nov. 2021, doi: 10.1109/TMTT.2021.3105413.

[26] G. Guzman, F. Beteille, R. Morineau, and J. Livage, “Electrical switching in VO_2 sol–gel films,” *J. Mater. Chem.*, vol. 6, no. 3, pp. 505–506, 1996, doi: 10.1039/JM9960600505.

[27] W. A. Vitale et al., “Field-enhanced design of steep-slope VO2 switches for low actuation voltage,” in *Proc. 46th Eur. Solid-State Device Res. Conf. (ESSDERC)*, Sep. 2016, pp. 352–355, doi: 10.1109/ESSDERC.2016.7599659.

[28] L. Xiao et al., “Fast adaptive thermal camouflage based on flexible VO_2/Graphene/CNT thin films,” *Nano Lett.*, vol. 15, no. 12, pp. 8365–8370, 2015, doi: 10.1021/acs.nanolett.5b04090.

[29] C. Ko and S. Ramanathan, “Stability of electrical switching properties in vanadium dioxide thin films under multiple thermal cycles across the phase transition boundary,” *J. Appl. Phys.*, vol. 104, no. 8, 2008, Art. no. 86105, doi: 10.1063/1.3000664.

[30] J. Jian, A. Chen, Y. Chen, X. Zhang, and H. Wang, “Roles of strain and domain boundaries on the phase transition stability of VO_2 thin films,” *Appl. Phys. Lett.*, vol. 111, no. 15, 2017, Art. no. 153102, doi: 10.1063/1.4991882.

[31] B. Hu et al., “Failure and reliability analysis of a SiC power module based on stress comparison to a Si device,” *IEEE Trans. Device Mater. Rel.*, vol. 17, no. 4, pp. 727–737, Dec. 2017, doi: 10.1109/tdmr.2017.2766692.

[32] S. Mueller, J. Muller, U. Schroeder, and T. Mikolajick, “Reliability characteristics of ferroelectric Si:HfO_2 thin films for memory applications,” *IEEE Trans. Device Mater. Rel.*, vol. 13, no. 1, pp. 93–97, Mar. 2013, doi: 10.1109/tdmr.2012.2216269.

[33] Y. Zhao et al., “Structural, electrical, and terahertz transmission properties of VO_2 thin films grown on c-, r-, and m-plane sapphire substrates,” *J. Appl. Phys.*, vol. 111, no. 5, 2012, Art. no. 53533, doi: 10.1063/1.3692391.